On the excitation mechanism of sub-second pulses of the 2011 August 10 solar flare

H. Mészárosová[1], L. Kashapova[2], S. Tokhchukova[3], and J. Rybák[4]

[1] Astronomical Institute of the Academy of Sciences of the Czech Republic, CZ–25165 Ondřejov, Czech Republic
[2] Institute of Solar-Terrestrial Physics SB RAS, Irkutsk, Russia
[3] Special Astrophysical Observatory of RAS, St.Petersburg Department, Russia
[4] Astronomical Institute of the Slovak Academy of Sciences, SK–05960 Tatranská Lomnica, Slovak Republic

ABSTRACT

Context. The subsecond pulses observed in microwaves during the solar flares are usually associated with the primary energy release processes. Observations and interpretations of these phenomena are important diagnostics method of processes in flare plasma. We present result of analysis of sunsecond pulses occurred during the C2.4 flare during 9:33:57–9:35:07 UT. This event was simultaneously observed by RATAN-600 and the Siberian Solar Radio Spectropolarimeter, Radioastrophysical observatory ISTP SB RAS.
Aims. The aim of the study is to find evidence of one or the other processes caused the observed phenomenon applying of numerical simulations based on plasma parameters obtained from observations.
Methods. The plasma parameters of the flare loops were obtained on the base of X-ray observations by the FERMI and RHESSI instruments. The topology and characteristic values of the magnetic field were determined according to the HMI/SDO and AIA/SDO observations. On the next step of the study, all these physical parameters were improved using the simulations of the microwave emission. We note that the simulation results gotten for the different approaches showed good agreement. The wavelets analysis of the dynamic spectrum with sub-second resolution at 26 frequencies (within 3797-8057 MHz) was carried out. The obtained wavelets patterns were compared with the patterns simulated for the models of the slab and current sheet.
Results. We revealed that this complex radio spectrum consist of sub-second pulsations, different burst groups and different continua (frequency drifts of 390 and 129 MHz/s). Origination of the one of the group could be associated with the density slab (loop) and the other one could arise in the current sheet. The analysis found the signatures of fast magnetoacoustic waves characteristic for both groups. The wavelet signatures in the observed radio spectrum are discussed from the point of the characteristic physical parameters of the loops and plasma emission mechanism as the most likely mechanism of the pulse origination.

Key words. Sun: flares – Sun: corona – Sun: radio radiation – Sun: oscillations

1. Introduction

The fine structure of radio emission of flares is studied during several decades. The main reason of these efforts is that observations and interpretations of this phenomenon is effective diagnostics of processes in flare plasma. The subsecond pulses (SSPs) are observed as intensive radio emission pulses with a subsecond duration which are overlaid on longer radio burst (Fleishman & Melnikov 1998, l999). These phenomena are observed during the impulse phase of solar flares and are associated with the primary energy release processes. SSPs are usually accompanied by a hard X-ray (HXR) bursts with the energy above 25–30 keV (e.g. Aschwanden & Güdel 1992). However, unambiguous correlation between these emissions is not generally observed.

There are two possible reasons of observed emission fragmentation. First of all, it could be result of the fragmentation of the primary energy release itself. It means that an individual pulses corresponds to a single event of the energy release or a particle acceleration. This scenario was used for explanation of the observed bursts by (Meshalkina et al. 2004, 2012).

Nevertheless, the observed fragmentation of radio emission could be a feature of the radiation mechanism or could be a result of the secondary fragmentation of the source emission structure. There are two mechanisms associated with the secondary fragmentation – the electron cyclotron maser and the plasma mechanism. Realization of the electron cyclotron maser mechanism needs high plasma density and strong magnetic field (Fleishman & Melnikov 1998, Fleishman 2004). We assume under plasma mechanism a double-stage process. At the first stage, the source generates oscillations which are unable to leave the plasma. It could be Langmuir waves, for example. The emission observed in radio range is result conversion (the second stage) of these oscillations into fast transverse electromagnetic waves (Fleishman & Melnikov 1998). The application of suggested models describing the different scenarios to explanation of observed SSPs allows to diagnose the processes of energy release and transfer in solar flares qualitatively as well as quantitatively.

Furthermore, radio spectra observed during solar flares might be complex, i.e. with many bursts and fine structures (e.g. Jiřička et al. 2001). One of possibilities how to study these fine structures in detail is the separation method (Mészárosová et al. 2011a) based on the wavelet analysis techniques. This method divides a complex radio spectrum into more spectra of simple bursts to simplify their analysis. This allows us to study radio spectra in more details either for such events when original radio spectrum (i) consists of a mixture of fine structures/bursts observed at the same frequencies and during the same time interval and therefore individual temporal/frequency components are difficult to recognize; (ii) when weaker bursts of radio spectrum coincide with stronger ones, e.g. with radio continua; (iii) when we want to locate possible fast sausage magnetoacoustic waves propagating in situ of radio spectrum source.

Properties of these impulsively generated MHD sausage magnetoacoustic waves propagating along their waveguide (e.g. coronal loop as a structure with enhanced plasma density). These waves were theoretically predicted by Roberts et al. 1983, 1984 and they exhibit periodic, quasiperiodic, and decay phases (Roberts et al. 1984). Because of a dispersion nature of these waves the quasiperiodic phase is generally stronger in amplitude and shorter in periods than the earlier periodic phase. Each of these fast magnetoacoustic waves form wave trains propagating along their waveguide and their time evolution were studied numerically in Nakariakov et al. (2004). They found that theese spectra form tadpole wavelet patterns with a narrow tail that precedes a broadband head. Then the periodic and quasiperiodic phases (Roberts et al. (1984) correspond to the tadpole tail and head, respectively. The start of decay phase corresponds to the tadpole head maximum.

In solar radio observations, these wavelet tadpoles were recognized, e.g. in the gyrosynchrotron radio burst (Mészárosová et al. 2009a; tadpoles detected at the same time over the whole frequency range), in dm-radio fiber bursts generated by the plasma emission processes (Mészárosová et al. 2009b, 2011b; slowly drifted tadpoles corresponding with the frequency drift of the whole group of fiber bursts), and in sources of narrowband dm-radio spikes (Karlický et al. 2011). The found wavelet tadpoles in Mészárosová et al. (2013) indicate the presence of fast magnetoacoustic waves propagating in the fan structure of the coronal magnetic null point.

These studies were supported by MHD numerical simulations made by e.g., Jelínek & Karlický (2012) (an increase in the distance between the initial perturbation and the detection point increases the length of the tadpole tail) and in Pascoe et al. 2013 (used a 2D numerical simulation model of the magnetoacoustic waveguide to consider the effects of an expanding magnetic field). An extended 2D MHD parametric investigation of wave processes in a density slab and a Harris current sheet was studied in Mészárosová et al. (2014) with respect to e.g., additional features superimposed on the basic tadpole wavelet spectrum.

Thus, a comparison of the separation method with wavelet analysis of observed bursts and MHD numerical models of the fast magnetoacoustic wave trains allows more precisely interpreting observational data and estimating flare plasma parameters. The target of our study is to find out a likely explanation of the microwave subsecond pulses occurred during the C2.4 class flare.

This paper is organized as follows. In Section 2 we describe the observed radio event with the subsecond pulses (SSPs) obtained by the different instruments and previous results of its analysis. Section 3 presents our detail analysis of the of the radio spectra with the SSPs and their characteristic properties. In Section 4 we studied flare loop topology and event magnetic fields with a help of spatial data observations. Finally, the results are summarized and discussed in Section 5.

2. Observations of the 2011 August 10 solar flare with the microwave subsecond pulses (SSPs)

Our solar microwave event under study were observed at 9:33:57–9:35:07 UT on 2011 August, 2011 during the GOES C2.4 flare occurred in the region AR NOAA 11236. The fine structures with the subsecond pulses (SSPs) vere detected in the event radio dynamic spectrum in the frequency range 3797–8057 GHz simultaneously with the RATAN-600 radio telescope (Pariiskii et al. 1976) and the Badary Broadband Microwave Spectropolarimeter (BBMS; Zhdanov & Zandanov 2011, 1015). The spectral resolution of RATAN-600 ($\Delta f/f$, where f is frequency) is 3% in the mean and the time resolution is 0.014 s. Dynamic spectra by BBMS were obtained with the same spectral resolution and 0.011 ms time resolution. Note, that it was for the first time when the SSPs were detected in the RATAN-600 data (Kashapova at al. 2013b). This is possible due to the upgrade of the spectral and polarization high-resolution receiver system in 2010 (Bogod et al. 2011). The solar radio emission was registered with RATAN-600 using the right- (RCP) and left-hand (LCP) circularly polarized antenna feeds displaced by the equal distance from focus. The Sun passed through the RCP and LCP beams with a 2.52 s delay, forming the one-dimensional imaging data of RATAN-600. The convolution of gaussian-like horizontal beam patterns of 30"–60" width with the flaring and pulsating sources give us the time profiles of SSPs smoothed with two spaced gaussian envelopes. Combined with the undistorted BBMS time profiles, one can derive the distance of SSPs source from the maximum of the background flaring source, which coincides with the position of the beam center. Thus, the detection of SSPs is possible only when the pulses occur while the source is passing through the narrow RATAN-600 beam. Position of background flaring source at 5.7 GHz was obtained by using the Siberian Solar Radio Telescope (SSRT) observations at 5.7 GHz (Grechnew et al. 2003).

This radio event under study were also observed by the by the Gamma-Ray Burst Monitor (GBM) of the Fermi Gamma-ray Space Telescope (Meegan et al. 2009) and by The Reuven Ramaty High-Energy Solar Spectroscopic Imager (RHESSI; Lin et al. 2002) – hard X-rays (HXR) observations with energies above 25 keV. To analyze a topology of flaring loops we used: (i) The EUV images observed by the Atmospheric Imaging Assembly (AIA) on the Solar Dynamics Observatory (SDO) (Boerner et al. 2012) and (ii) the magnetograms observed by the Helioseismic and Magnetic Imager (HMI/SDO; Schou et al. 2012). Our 3D magnetic field reconstruction was based on HMI/SDO data. Result of 3D magnetic field reconstruction was imported into widget of GX_Simulator software (Nita et al. 2011). This widget was used for both the simulation of gyrosynchrotron (GS) emission and the flare loop topology analysis.

includegraphics[width=9.0cm, height=8cm]f01n2.eps

Fig. 1. Separation of bursts of the 2011 April 10 event: (a) original radio dynamic spectrum with broadband pulses lasted 70 s (9:33:57–9:35:07 UT, frequency range = 3797–8057 MHz), (b) averaged global wavelet spectrum (AGWS) made from the spectrum in the panel a with important peaks for the periods P= 2.35, 4.64, 16.68, and 30.30 s (arrows in blue) and with local minima for the periods 0.07, 1.49, 3.03, 5.83, 21.54, and 40.26 s (arrows in red).

We used the same 3D extrapolation data cube and a model of flare loop as in Kashapova et al.(2013a).

The former analysis of HXR and microwave (MW) radio emission revealed that the temporal profiles of the 6–12 keV and 30–50 keV HXR energy bands reached the maximum at the same time (Kashapova et al. 2013a). This fact indicated the flare plasma heating without a main role of the accelerated electron injection and assumed presence high-temperature source located directly in the place of energy release. Results of a comparison of the simulated MW gyrosynchrotron spectrum with different models computed for the observed MW spectrum indicated that the observed emission was excited by the electron flux with the thermal velocity distribution (TE about 40 MK) in the small loop with weak magnetic field (about 50 G).

The HXR data observed by the GMB/FERMI allowed to carried out study of a relation between the fine structure of the SSPs and the HXR emission variations with sub-second cadence (see Kashapova et al.2013b). The analysis also did not confirm significant effect of accelerated electron beams on a fragmentation of the microwave emission.

3. Detail analysis of the radio dynamic spectrum with the SSPs and their characteristic properties

Firstly, we analyze the SSRP radio dynamic spectrum with a respect to individual types of observed bursts and their physical parameters. We also search for a possible presence of the propagating fast magnetoacoustic waves.

3.1. Separation of the individual bursts of the radio dynamic spectrum

The original radio dynamic spectrum with broadband subsecond pulses is shown in panel a of Fig. 1. This event lasted 70 s (9:33:57–9:35:07 UT) and was observed in the frequency range = 3797–8057 MHz with time resolution of 0.011 s.

To reveal individual bursts presented in this radio dynamic spectrum we used a separation method (Mészárosová et al. 2011a) based on the wavelet analysis technique. This method divides the original complex radio spectrum into two or more simple bursts to simplify their analysis and study separated individual radio spectra in more details. This method is convenient in our case because the original radio spectrum under study consists of a mixture of different radio bursts observed at the same frequencies and during the same time interval. This causes that individual possible temporal components are difficult or impossible to recognize them in the original spectrum. Moreover, this method enables us to reveal weaker radio bursts of the original radio spectrum that coincide with stronger ones, e.g. with radio continua. Futhermore, time series of the separated dynamic spectra enables easier detection of the fast magnetoacoustic waves propagating in situ of the radio source under study (Section 3.2.).

In our case, we used the method of separation of the original radio spectrum according to the temporal periods (see more detail method description in Mészárosová et al. 2011a). We computed an average global wavelet spectrum (AWGS) from all time series of the original spectrum in the panel 1a of Fig. 1. This AWGS curve is diplayed in panel b (Fig. 1). There are shown important peaks for the periods P= 2.35, 4.64, 16.68, and 30.30 s (blue arrows) as well as individual local minima with their periods 0.07, 1.49, 3.03, 5.83, 21.54, and 40.26 s (red arrows).

Then we computed new individual radio dynamical spectra but each of them for only selected period range of the charcteristic peak period. For example, we can be interested only in bursts with a dominant temporal period ≈16.68 s. Then we compute new radio dynamic spectrum for bursts with their time series in the period range 5.83–21.54 s (see panel b, Fig. 1). Such a new separated spectrum is displayed in panel 4a of Fig. 2. All new separated spectra are computed via the inverse wavelet method (e.g. Torrence & Compo, 1998). Overview of all new separated bursts is presented in Fig. 2 (panels 1a–6a). The individual characteristic types of bursts are separated in the period ranges of 0.07–1.49 s (panel 1a, subsecond pulses), 1.49–3.03 s (panel 2a), 3.03–5.83 s (panel 3a), 5.83–21.54 s (panel 4a), 21.54–40.26 s (panel 5a), and for all periods > 40.26 s. Arrows in panels 5a–6a show frequency drifts of bursts (see Table 1). The positive and negative parts of amplitudes (in relation to their mean values) are given in white and black, respectively (panels 1a–6a). The period range < 0.07 s (panel b, Fig. 1) belong to instrument interferences.

The reason of the separation is showed in panels 1b–6b (Fig. 2). There are compared selected individual time series of the original radio dynamic spectrum (in red) as well as of the separated one (in green) always at the same frequency 5194 MHz. We can see that the separated individual peaks (in green) in the panel 1b belong only to the subsecond pulses. The separated individual peaks in the panel 2b–4b reflect the different groups of pulses (their small onsets) without their frequency drift. Finally, the separated peaks in the panel 5b–6b show various types of continua (their data onsets) with significant fequency drifts - see Table 1. The bursts presented in panels 1–6 (Fig. 2) are not be visible in the original radio spectrum. (Note: selected time interval in panel 1b is 49–59 s of the entire 70 s event duration). Frequency drifts (arrows 1, 2, and 3; panel 5a) fd = 519.8, 138.4, and -261.8 MHz s^{-1}, respectively. Frequency drift (arrow 4, panel 6a) fd = 215 MHz s^{-1}.

We used the density model of Aschwanden & Benz (1995) with numerical values of height $h1$ = 1.6×102 Mm, density of the quiet corona n_Q = 4.6×108 cm−3, and the parameter p = 2.38. Thus, we obtained the average electron densities at mean coronal altitudes with plasma velocities (and other parameters) for individual bursts. These characteristic parameters of the radio bursts are shown in Table 1.

3.2. Propagating fast magnetoacoustic waves in the SSRP radio dynamic spectrum

We selected individual parts of time series of the separated radio dynamic spectrum of panel 1a (Fig. 2). These time se-
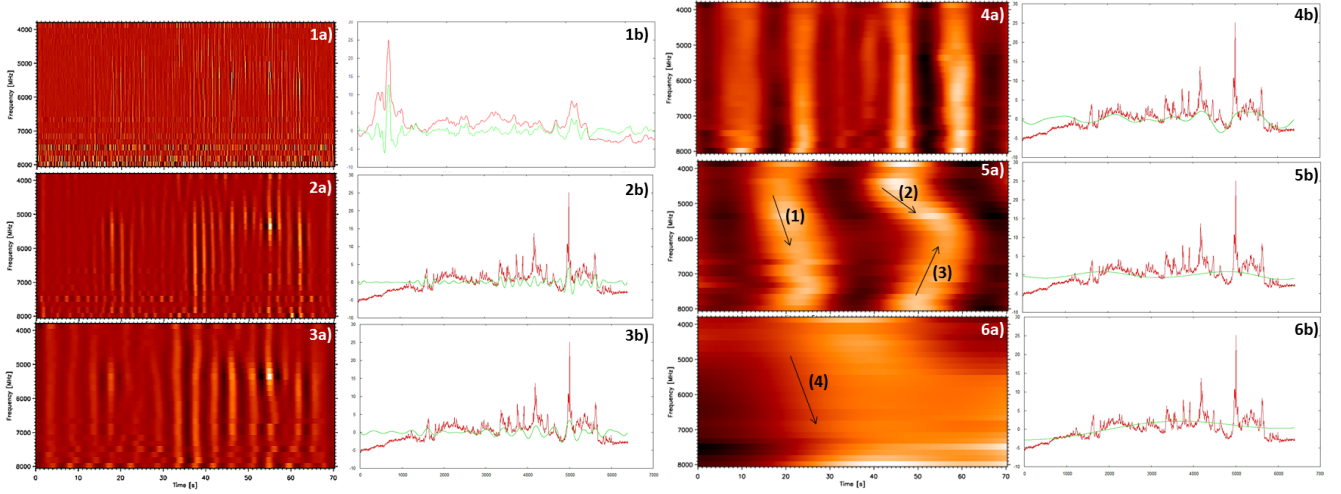
Fig. 2. Separated bursts (panels 1a–6a) and their selected time series (panels 1b–6b) of the original radio dynamic spectrum in Fig. 1a. Bursts are separated in the period ranges of 0.07–1.49 s (panel 1a), 1.49–3.03 s (panel 2a), 3.03–5.83 s (panel 3a), 5.83–21.54 s (panel 4a), 21.54–40.26 s (panel 5a), and for all periods > 40.26 s. Arrows in panels 5a–6a show frequency drifts of bursts (see Sect. 3.2). The positive and negative parts of amplitudes (in relation to their mean values) are given in white and black, respectively (panels 1a–6a). Reason of the separation is showed in panels 1b–6b with comparing of peaks between the time series of the original radio dynamic spectrum (in red) and the separated one (in green) always at the same frequency 5194 MHz – see Sect. 3.2. (Time in panel 1b is 49–59 s of the 70 s event duration). Frequency drifts (arrows 1, 2, and 3; panel 5a) $fd = 520, 138,$ and -262 MHz s^{-1}, respectively. Frequency drift (arrow 1, panel 6a) $fd = 215$ MHz s^{-1}.

Table 1. Characteristic parameters of the radio bursts with a frequency drift FD, where dur = duration, v_p = plasma velocity, B = magnetic field strength, SF & EF = starting & ending frequency, ST & ET = starting & ending time, $S\rho$ & $E\rho$ = starting & ending averaged electron density, and SA & EA = starting & ending mean coronal altitudes, respectively.

Fig. No.	Arrow No.	SF [MHz]	EF [MHz]	ST [s]	ET [s]	dur [s]	FD [MHz s^{-1}]	$S\rho$ [cm^{-3}]	$E\rho$ [cm^{-3}]	SA [Mm]	EA [Mm]	v_p [km s^{-1}]	B [G]
2	1	4408	5744	17.37	19.94	2.57	519.8	2.41×10^{11}	4.09×10^{11}	4.24	3.39	329.03	79.56
2	2	4408	5744	41.39	51.04	9.65	138.4	2.41×10^{11}	4.09×10^{11}	4.24	3.39	87.63	21.19
2	3	6073	7607	50.63	44.77	5.86	261.8	4.57×10^{11}	7.18×10^{11}	3.24	2.68	95.30	31.75
2	4	4289	5194	32.74	36.95	4.21	215.0	2.28×10^{11}	3.34×10^{11}	4.34	3.69	153.13	36.03
3	1	4887	5957	61.76	62.13	0.37	2891.9	2.96×10^{11}	4.00×10^{11}	3.89	3.29	1610.38	431.72

ries and their wavelet tadpole patterns with characteristic period $P \approx 0.7$ s are presented in panels a–d of Fig. 3. These time series (9:34:56–9:35:01 UT) observed at frequencies 4887, 5579, 5957, and 6073 MHz have their peak maxima (red arrows) equal to maxima of the wavelet tadpole heads. Average frequency drift of these heads maxima $fd = 2892$ MHz s−1. These wavelet patterns are a signature of a presence of propagating fast magnetoacoustic waves.

Detail for time interval of 9:34:56–9:35:02 UT of the original radio dynamic spectrum (panel a, Fig. 1) shows individual reverse III-type bursts (Fig. 4) with the average frequency drift $fd = 2892$ MHz s^{-1}, i.e. the same frequency drift as the maxima of the wavelet tadpole heads.

Selected time series of the separated radio dynamic spectrum in panel 2a (Fig. 2) and their wavelet tadpole patterns with characteristic period $P \approx 2$ s are presented in Fig. 5. These time series (9:34:51–9:35:07 UT) observed at frequencies 5026, 5398, 5579, and 6593 MHz have their peak maxima (red arrows) equal to maxima of the wavelet tadpole heads. There is no measurable frequency drift of the tadpole head maxima. These wavelet patterns are also a signature of a presence of propagating fast magnetoacoustic waves.

4. The flare loops topology and magnetic with a help of spatial data observation

Now we studied the SDO/AIA/HMI data to know flare loops topology as well as the FERMI and RHESSI hard X-rays data to obtain more detailed information e.g. about magnetic field line configurations.

As a peculiarity of this event there were detected also hard X-rays (HXR) flux with energies above 25 keV that is not typical for weak C-class flares (2013GeAe..53.1021K). A good correlation between the HXR and microwave time profiles was found which indicated the generation of both HXR and MW emission by common population of electrons. Plasma parameters were obtained using the FERMI HXR spectra fitting. Using these parameters the RATAN-600 microwave spectra of the background flaring source were simulated. It was revealed that the flare emission as well as the subsecond pulses were generated by a high temperature source T ¿ 30 MK 2013GeAe..53.1021K. In this study the plasma parameters of flare loops were obtained from the X-ray observations by FERMI and RHESSI instruments. SDO AIA and HMI data were used for obtaining the topology of flaring loops and characteristic values of magnetic fields.
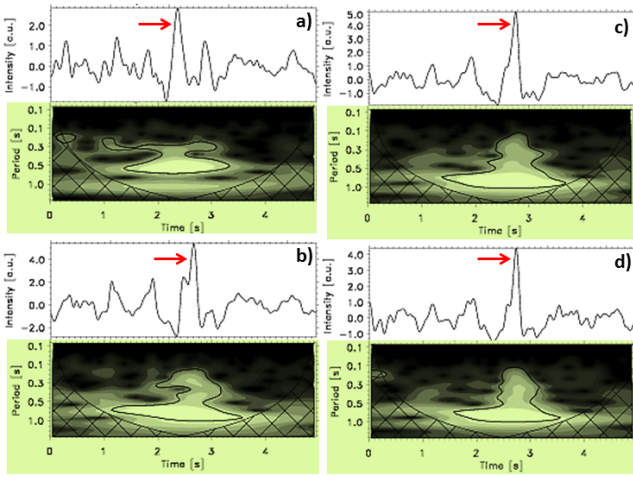
Fig. 3. Panels *a–d*: Selected time series of the separated radio dynamic spectrum in panel 1*a* (Fig. 2) and their wavelet tadpole patterns with characteristic period $P \approx 0.7$ s. These time series (9:34:56–9:35:01 UT) observed at frequencies 4887, 5579, 5957,
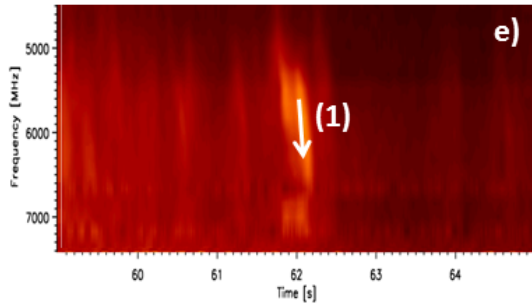

Fig. 4. Detail (9:34:56–9:35:02 UT) of the original radio dynamic spectrum (panel *a*, Fig. 2) with individual reverse III-type bursts with the average frequency drift $fd = 2892$ MHz s^{-1}.
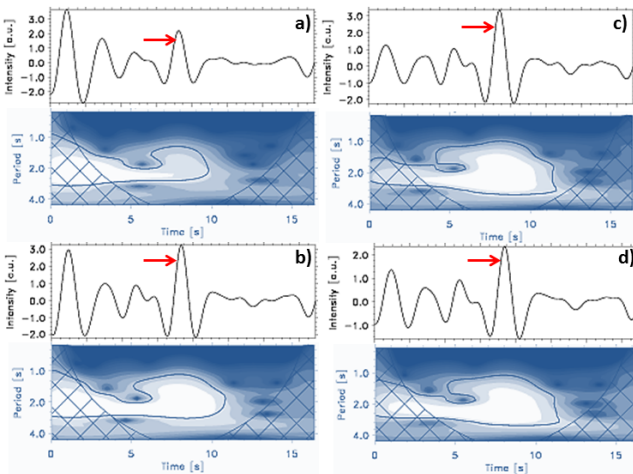

Fig. 5. Selected time series of the separated radio dynamic spectrum in panel 2*a* (Fig. 2) and their wavelet tadpole patterns with characteristic period $P \approx 2$ s. These time series (9:34:51–9:35:07 UT) observed at frequencies 5026, 5398, 5579, and 6593 MHz have their peak maxima (red arrows) equal to maxima of the wavelet tadpole heads. There is no measurable frequency drift of the tadpole head maxima.

Fig. 6. Structure of flaring loops displayed by using 131 Å image obtained at 09:34 UT and overlaid by X-ray sources at the different energy bands showed as contours. These X-ray contours were constructed for the same time moment with one minute exposition.

Fig. 7. The rotated negative image of the flare loops (94 Å image obtained at 09:34 UT). The blue and red lines show the example of measurement of height and radius of the loop.

Fig. 8. Rotated 3D model of magnetic file obtains from potential extrapolation.

Fig. 9. Model.

fig 05 Structure of flaring loops displayed by using 131 Å image obtained at 09:34 UT and overlaid by X-ray sources at the different energy bands showed as contours. These X-ray contours were constructed for the same time moment with one minute exposition.

fig06 The rotated negative image of the flare loops (94 Å image obtained at 09:34 UT). The blue and red lines show the example of measurement of height and radius of the loop.

fig07 Rotated 3D model of magnetic file obtains from potential extrapolation.

5. Discussion and conclusions

1. We revealed that the 3797-8057 MHz dynamic radio spectrum consists of sub-second pulsations of the burst groups and continua (frequency drifts of 390 and 129 MHz/s).
2. Origination of one of the groups could be associated with the density loop and the other one could arise in a current sheet
3. We found the signatures of fast magnetoacoustic waves characteristic for both of the groups.

References

Aschwanden, M. J., & Benz, A. O. 1995, ApJ, 438, 997
Aschwanden, M. J., & Güdel, M. 1992, ApJ, 401, 736
Boerner, P., Edwards, C., Lemen, J., et al. 2012, Sol. Phys., 275, 41
Bogod, V. M., Alesin, A. M., & Pervakov, A. A. 2011, Astrophysical Bulletin, 66, 205
Fleishman, G. D., & Melnikov, V. F. 1998, Soviet Physics Uspekhi, 41, 1157
Fleishman, G. D., & Melnikov, V. F. 1999, in ESA Special Publication, Vol. 448, Magnetic Fields and Solar Processes, ed. A. Wilson, et al., 1247
Fleishman, G. D. 2004, ApJ, 601, 559

Fig. 10. Model.

Grechnev, V. V., Lesovoi, S. V., Smolkov, G. Y., et al. 2003, Sol. Phys., 216, 239

Jelínek, P., & Karlický, M. 2012, A&A, 537, A46

Jiřička, K., Karlický, M., Mészárosová, H., & Snížek, V. 2001, A&A, 375, 243

Karlický, M., Jelínek, P., & Mészárosová, H. 2011 A&A, 529, A96

Kashapova, L. K., Tokhchukova, S. K., Rudenko, G. V., Bogod, V. M., & Muratov, A. A. 2013a, Cent. Eur. Astrophys. Bull., 37, 573

Kashapova, L. K., Tokhchukova, S. K., Zhdanov, D. A., Bogod, V. M., & Rudenko, G. V. 2013b, Geomagnetism and Aeronomy, 53, 1021

Lin, R. P., Dennis, B. R., Hurford, G. J., et al. 2002, Sol. Phys., 210, 3

Meegan, C., Lichti, G., Bhat, P. N., et al. 2009, ApJ, 702, 791

Meshalkina, N. S., Altyntsev, A. T., Sych, R. A., Chernov, G. P., & Yihua, Y. 2004, Sol. Phys., 221, 85

Meshalkina, N. S., Altyntsev, A. T., Zhdanov, D. A., et al. 2012, Sol. Phys., 280, 537

Mészárosová, H., Karlický, M., Rybák, J., & Jiřička, K. 2009a, ApJ, 697, L108

Mészárosová, H., Karlický, M., Rybák, J., & Jiřička, K. 2009b, A&A, 502, L13

Mészárosová, H., Rybák, J., & Karlický, M. 2011a, A&A, 525, A88

Mészárosová, H., Karlický, M., & Rybák, J. 2011b, Sol. Phys., 273, 393

Mészárosová, H., Dudík, J., Karlický, M., et al. 2013, Sol. Phys., 283, 473

Mészárosová, H., Karlický, M., Jelínek, P., & Rybák, J. 2014, ApJ, 788, 44

Nakariakov, V. M., Arber, T. D., Ault, C. E., et al. 2004, MNRAS, 349, 705

Nita, G. M., Fleishman, G. D., Gary, D. E., Kuznetsov, A. A., & Kontar, E. P. 2011, in AAS/Solar Physics Division Abstracts 42, 1811

Pariiskii, I. N., Korolkov, D. V., Shivris, O. N., et al. 1976, AZh, 53, 1017

Pascoe, D. J., Nakariakov, V. M., & Kupriyanova, E. G. 2013, A&A, 560, A97

Roberts, B., Edwin, P. M., & Benz, A. O. 1983, Nature, 305, 688

Roberts, B., Edwin, P. M., & Benz, A. O. 1984, ApJ, 279, 857

Schou, J., Scherrer, P. H., Bush, R. I., et al. 2012, Sol. Phys., 275, 229

Torrence, C., & Compo, G. P. 1998, Bull. Am. Meteorol. Soc., 79, 61

Zhdanov, D. A., & Zandanov, V. G. 2011, Central European Astrophysical Bulletin, 35, 223

Zhdanov, D. A., & Zandanov, V. G. 2015, Sol. Phys., 290, 287